ISSN 2616-5767 Vol.7, Issue 3: 29-38, DOI: 10.25236/AJETS.2024.070305

Lidar SLAM-Enabled Precision Detection of Coal Bunker Structural Damage

Jingxuan Yan[1,*], Kejun Huang[2], Xiaoquan Huo[3]

[1]*Xi'an Tieyi High School, Xi'an, Shaanxi, 710054, China*
[2]*Shaanxi Engineering Research Center for Intelligent Coal Mine, Xi'an, Shaanxi, 710054, China*
[3]*Shaanxi Coal Tongchuan Mining Co. Ltd., Tongchuan, Shaanxi, 727000, China*
yanjingxuan2025@163.com
[*]*Corresponding author*

Abstract: *Efficient repair of structural damage in coal bunkers is crucial for minimizing economic losses in mining operations. Current repair practices often face challenges like poor visibility and high risk. This study proposes a novel solution using lidar SLAM(simultaneous localization and mapping) technology with the ICP (iterative closest point) algorithm to address these challenges, aiming to enhance safety and efficiency in coal bunker repairs. A specialized detection system is designed for coal bunker exploration robots, integrating 3D visualization software for real-time monitoring, attitude adjustment, and cross-sectional surveillance. Key hardware components include a laser radar for precise scanning and balance sensors for stability. Extensive experimental trials on coal bunkers validate the system's exceptional precision, with key performance metrics such as ATE (absolute trajectory error) and RTE (relative trajectory error) consistently below 0.01, meeting the rigorous demands of bunker inspection. The system efficiently detects critical structural anomalies like protruding reinforcement bars and partial wall ruptures, issuing timely warnings for potential hazards. These results validate the system's robustness and accuracy in identifying and characterizing coal bunker damage, providing actionable guidelines for safe, efficient, and technologically advanced bunker inspections.*

Keywords: *ICP; Lidar SLAM; Coal Bunker Structural Damage Detection; 3D Scanning; Coal Storage Infrastructure Assessment*

1. Introduction

Coal bunkers are essential storage facilities for coal [1-2], comprising four main parts: an upper opening, body, lower opening, and coal discharge gate. While crucial for coal transportation, they face issues like wall adhesion, deformation, and blockages due to coal properties and construction factors [3-4]. Current underground bunkers rely heavily on manual labor, posing safety risks in hazardous working conditions. Enhancing bunker perception capabilities is vital for safety and operational efficiency, crucial for improving safety standards.

To improve the efficiency of removing adhesive condensate layers on coal bunker walls, enhance the perception capability of coal bunkers, and ensure the safety of clearance personnel, France's Standard Industries International developed the POWERNET and GIONET systems for efficient coal bunker cleaning. Pneumat Systems' BinWhip system tackles powder silo wall cleaning. Jingguo Ma and Zubang Li[5] proposed a coal level detection method, with limitations in underground bunkers. Kajzar V, Kukutsch R[6], used 3D laser scanning for coal mine stability monitoring. Quan Jiang, S Zhong[7], measured tunnel deformations with 3D laser scanning. Laser SLAM methods include graph optimization and filter-based approaches[8]. Distance-based methods like ICP[9] are for scan matching. Loop closure detection uses Monte Carlo node search and FPFH-based algorithms[10-14]. Back-end optimization includes C-T SLAM, BALM, and LIO-SAM[15-17]. The focus is on distance-based methods and 3D scanning systems[18].

This paper suggests using a 3D Lidar SLAM approach with the ICP algorithm for inspecting underground coal silos. It aims to address challenges in measuring material positions and monitoring silo deformations while ensuring dust penetration capability and measurement accuracy. This involves breaking through underground protection technology for 3D laser sensors and designing a lightweight sensor stabilization and scanning mechanism. Efficient measurement and comparison of coal silo inner wall features are achieved through rapid point cloud stitching and data storage algorithms. This enables

ISSN 2616-5767 Vol.7, Issue 3: 29-38, DOI: 10.25236/AJETS.2024.070305

timely detection and localization of cohesion and deformation issues, ensuring safe raw coal transportation.

2. Materials and Methods

2.1. The principle of two-dimensional digital measurements of coal bunkers

We adopt a short-range phase-shift laser rangefinder utilizing the digital phase measurement principle [19] for precise distance determination in coal bunker inspections. This approach calculates the distance based on the phase delay induced by a modulated laser signal traveling along the measurement path. The relationship between the phase delay, angular frequency ω, and distance is given by equation (2). Integrating this relationship into the basic distance formula (equation 1), we derive the distance expression (equation 3).

$$D = ct/2 \tag{1}$$

In the formula: D represents the distance between Points A and B.c represents the speed at which the laser propagates in the air.t represents the time required for one round trip from Sensor A to Point B on the coal bunker wall.

$$t = \varphi/\omega \tag{2}$$

$$D = 1/2ct = 1/2c \cdot \varphi/\omega = c/(4\pi f)(N\pi + \Delta\varphi) = c/4f(N + \Delta N) = U(N+) \tag{3}$$

In the formula: φ is the total phase delay generated by one round trip of the signal on the measuring line. ω is the angular frequency of the modulating signal. N is the number of half wavelengths of modulation contained in the measuring line. Δφ is the phase delay that is less than π from one round trip of the signal on the measuring line. ΔN is the decimal part of the modulated wave that is less than half a wavelength in the measuring line, where $\Delta N = \varphi/\omega$.

2.2. Construction of a Lidar SLAM graph optimization framework based on the ICP algorithm

2.2.1. Graph optimization framework construction

Our study employs a high-precision ICP (iterative closest point algorithm) to register 3D point clouds from continuous frames, keyframes, and loop closures. By incorporating constraints such as key poses, coal bin planes, and loop closures, we develop an optimized SLAM (simultaneous localization and mapping) graph specifically for coal bunker environments.[20]

The framework (Figure 1) consists of four parallel threads: Lidar odometry, plane constraint, loop constraint, and pose optimization. Input data includes 3D point clouds (blue arrows) and LiDAR odometry (black arrows), while red arrows indicate pose constraints during optimization. This process yields optimized pose information and denoised point cloud maps, with ICP initially employed for inter-keyframe registration and subsequently for refining keyframe poses, which serve as pose nodes in the SLAM graph.[21]

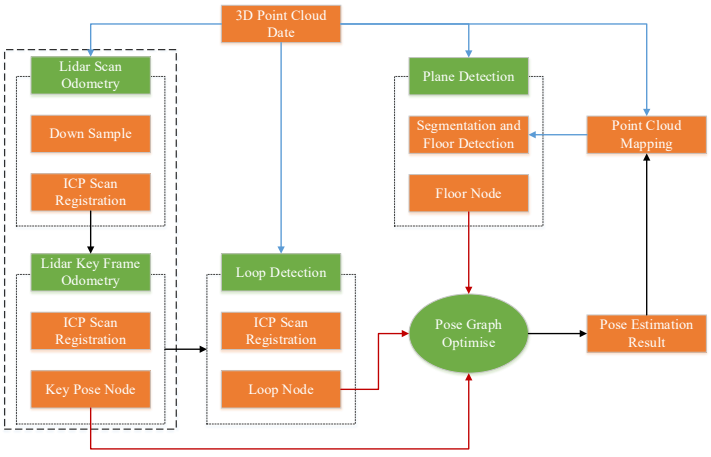

Figure 1: The iterative closest point and simultaneous localization and mapping system framework.

ISSN 2616-5767 Vol.7, Issue 3: 29-38, DOI: 10.25236/AJETS.2024.070305

2.2.2. Lidar attitude adjustment

The ICP algorithm aligns the incoming real-time point cloud with the previously acquired point cloud to determine the relative pose $\Delta T_{t-1,t}$ from t to $t-1$, where the position of the point cloud at time $t-1$ is T_{t-1}. Thus, the pose of the 3D laser scanner at time t can be computed using equation (4):

$$T_t = T_{t-1}\Delta T_{t-1,t} \tag{4}$$

By iteratively executing the ICP algorithm, the pose of a 3D laser scanner can be precisely established at any moment.[22]

Utilizing the odometry between consecutive frames, the pose of the $(k-1)$th keyframe, T_{k-1}, and the pose of the kth keyframe, T_k, can be derived using equation (5), yielding the relative transformation pose between sequential keyframes:

$$\Delta T_{k-1,k} = T_{k-1}^{-1}T_k = \begin{pmatrix} \Delta R & \Delta s \\ 0 & 1 \end{pmatrix} \tag{5}$$

Here, the Euclidean distance Δsk between consecutive keyframes is defined as $\Delta sk = ||T_k - T_{k-1}||$, and the rotation angle θk between them is given by $\theta k = \arccos(\text{dot}(T_k, T_{k-1}) / (||T_k|| * ||T_{k-1}||))$. The criterion for keyframe determination is typically based on a threshold for Δsk or θk, such as a minimum angular change or displacement.

2.2.3. Methods for point cloud construction

When selecting the $(k+1)-th$ frame as a keyframe, continuous keyframe optimization is performed using ICP. This yields the relative pose T_{k+1}^{l} between keyframes. Based on the poses T_k^w of k keyframes in world coordinates, the pose T_{k+1}^w of the $(k+1)-th$ keyframe in world coordinates can be obtained through coordinate transformation as $T_{k+1}^w = T_k^w \cdot T_{k+1}^1$. Finally, by using T_{k+1}^w, the coordinates of the $(k+1)-th$ keyframe's point cloud are transformed into the world coordinates as Q_{k+1}, and the point cloud map is updated using an octree structure. More details are shown in Figure 2.[23]

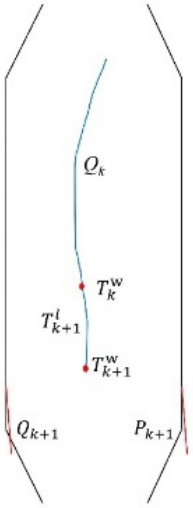

Figure 2: Point cloud map construction drawing.

The specific steps to suppress road point cloud noise are outlined below:

Step 1: Compute the normal vector using the line connecting the current tracking point and the preceding tracking point. Given two tracking points p_1 and p_2, the vector $v = p_2 - p_1$ defines the direction. The normal vector n is then found perpendicular to v. Using this normal vector, the plane equation at the trajectory point is calculated using equation (6), as depicted in Figure 3(a).

$$(x_2 - x_1)(x - x_2) + (y_2 - y_1)(y - y_2) + (z_2 - z_1)(z - z_2) = 0 \tag{6}$$

Step 2: Given a cross-section with a thickness δ, extract a point cloud strip with a width of 2δ on either side of the normal plane. This involves calculating the Euclidean distance from each point in the point cloud to the normal plane, subject to the condition expressed by equation (7).

ISSN 2616-5767 Vol.7, Issue 3: 29-38, DOI: 10.25236/AJETS.2024.070305

$$d_i \leq \frac{\delta}{2} \tag{7}$$

Step 3: Assuming the point cloud is lying on the same plane, project points the not on the plane to obtain a discrete point set on the normal plane, as shown in Figure 3(b).

Step 4: First, apply the RANSAC algorithm to robustly fit a curve; next, use the least squares method to refine the inlier fit, and finally, eliminate outliers from each segment, producing a denoised point cloud representation of the coal bunker section, as shown in Figure 3(c).

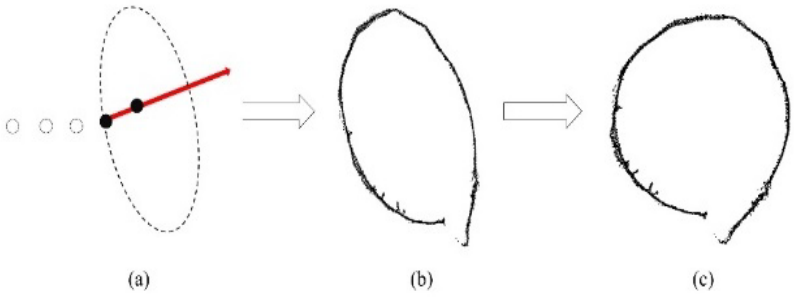

Figure 3: Coal bunker point cloud denoising flowchart.

Utilizing offline data processing and pose graph optimization techniques [24], initial registration results are refined to create an accurate 3D model of the coal bunker. By comparing this model with theoretical and historical data, the bonding layer's position can be identified, and bunker deformation quantified.

3. Coal bunker exploration experimental design

3.1. Coal bunker exploration robot design

The coal bunker exploration robot integrates hardware and software to form a 3D visualization system for analyzing bunker status and guiding repair efforts. Figure 4 presents the preliminary design of a coal bunker, measuring 46.48 meters in height, with a maximum east-west dimension of 10.57 meters and a maximum north-south dimension of 13.69 meters.

The robot is lowered into the bunker via ropes, equipped with laser sensors for wall scanning (Figure 5) and balance sensors for maintaining stability (Figure 6). Attitude graph optimization techniques are employed to correct initial registration results, with continuous acquisition of 3D data until the bunker bottom is reached. The robot is subsequently lifted back to the surface. Algorithms, combined with software, monitor and merge the 3D data, generating a 3D point cloud model of the coal bunker.

Figure 4: Initial design drawing of the coal bunker.

ISSN 2616-5767 Vol.7, Issue 3: 29-38, DOI: 10.25236/AJETS.2024.070305

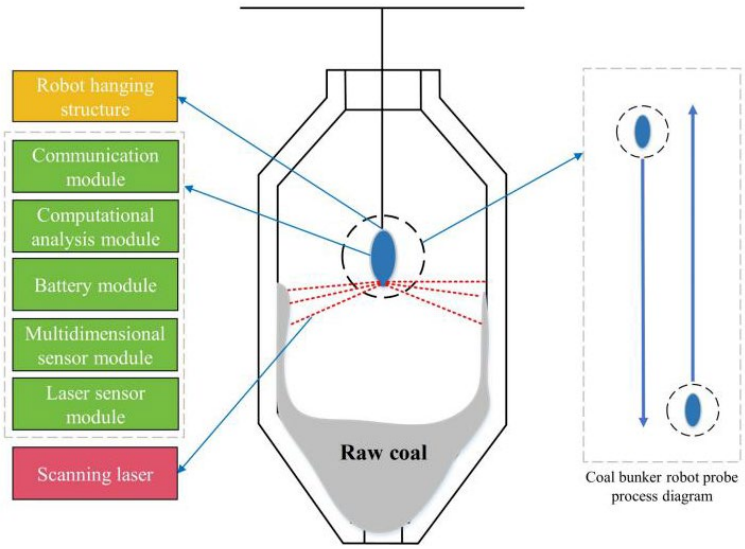

Figure 5: Exploration process diagram of the coal bunker robot.

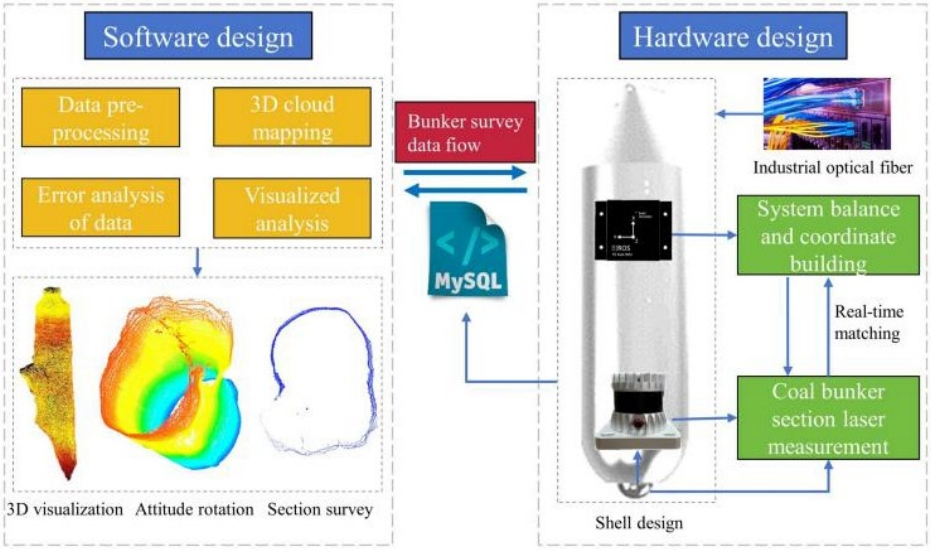

Figure 6: System design diagram.

3.2. Recognition of coal bunker damage

Following the initial experimental design, a coal bunker measurement software system is utilized for 3D reconstruction and rotation, enabling multi-angle visual analysis of strain distribution and damage morphology. Figure 7 and Figure 8 present texture maps of the experimental bunker.

Figure 7 depicts the current state texture map of the bunker generated by transferring the robot's measurement data to 3D visualization software, validating the effectiveness of both the robot and the software in confirming bunker shape and deformation extent. Figure 8 presents a multi-perspective rendering of the bunker's 3D point cloud based on reflectance intensity, aiding in evaluating bunker wall roughness and distinguishing materials like raw coal and rocks based on their reflectance intensities.

ISSN 2616-5767 Vol.7, Issue 3: 29-38, DOI: 10.25236/AJETS.2024.070305

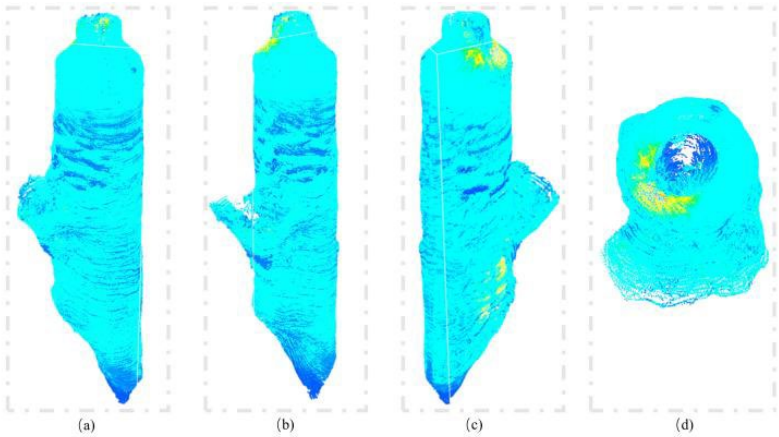

Figure 7: Three-dimensional point cloud map of the coal bunker.

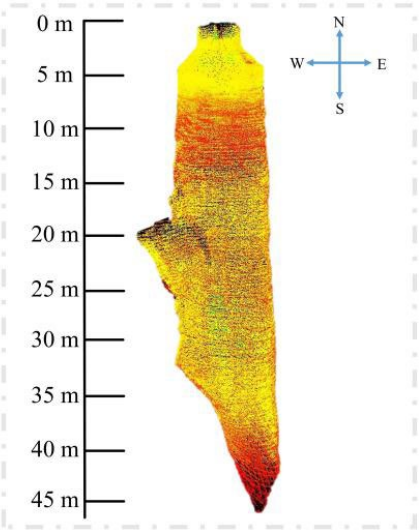

Figure 8: Three-dimensional point cloud rendering of a coal bunker from multiple perspectives based on the reflectance intensity.

4. Results and Discussion

This section presents the main findings of the coal bunker exploration experiments, focusing on the performance of the proposed detection system and its ability to accurately identify structural anomalies.

4.1. Performance Metrics

The ATE (absolute trajectory error) and RTE (relative trajectory error) serve as key indicators of the system's precision. Table 1 summarizes the ATE and RTE values for the six critical surfaces of the experimental coal bunker, the corresponding pictures are shown in Figure 9. Across all subplots, both ATE and RTE remain consistently below 0.01, demonstrating exceptional precision in the lidar SLAM-enabled detection system. These results meet the stringent requirements for bunker inspection, affirming the system's robustness and accuracy in identifying and characterizing coal bunker damage.

Table 1: Trajectory Error Measurement of the Coal Bunker

Error	ATE	RTE
Subplot(a)	0.03	0.03
Subplot(b)	0.070	0.059
Subplot(c)	0.071	0.073
Subplot(d)	0.029	0.08
Subplot(e)	0.06	0.06
Subplot(f)	0.09	0.048

ISSN 2616-5767 Vol.7, Issue 3: 29-38, DOI: 10.25236/AJETS.2024.070305

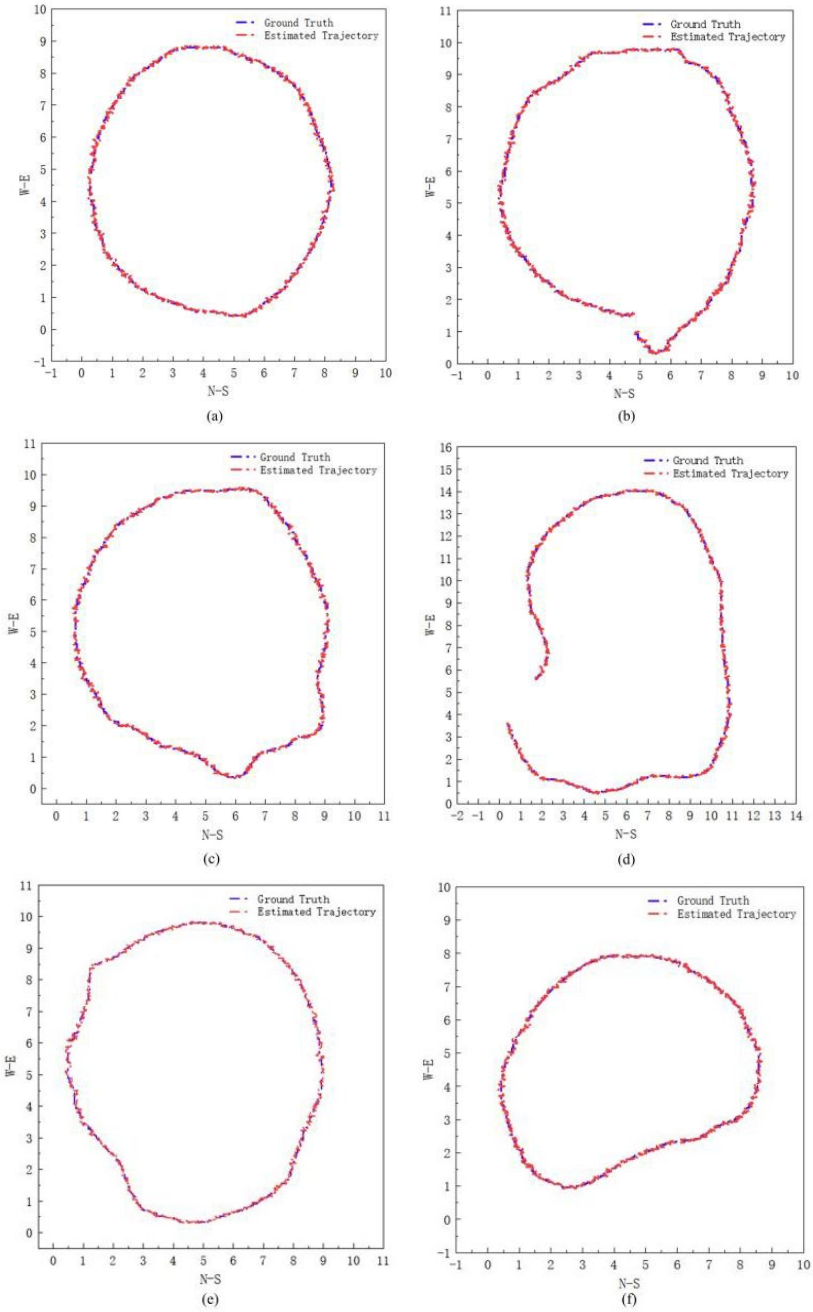

Figure 9: Comparison of the coal bunker point cloud data measurements.

4.2. Damage Detection and Characterization

The system effectively detects and characterizes various types of structural damage. Figure 10-13 illustrates the detection of protruding reinforcement bars, a common hazard in coal bunkers. The system accurately locates and alerts operators to these potential safety risks, enabling timely intervention. Similarly, partial wall ruptures, another critical anomaly, are accurately detected. These results validate the system's ability to identify subtle structural changes and provide actionable information for maintenance and repair.

ISSN 2616-5767 Vol.7, Issue 3: 29-38, DOI: 10.25236/AJETS.2024.070305

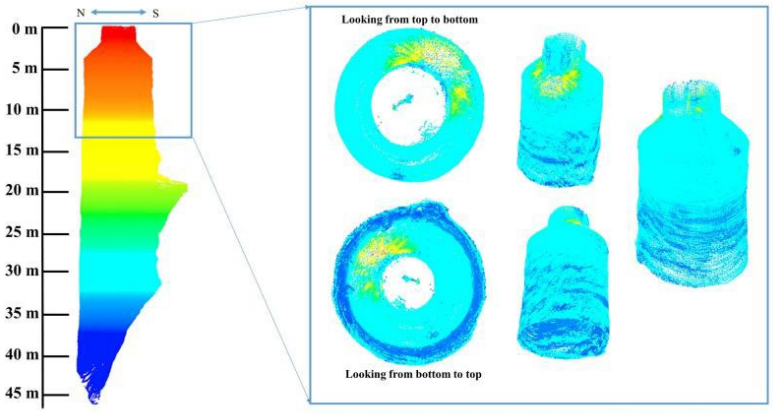

Figure 10: Multi-angle view of the intact area of the upper structure of the coal silo.

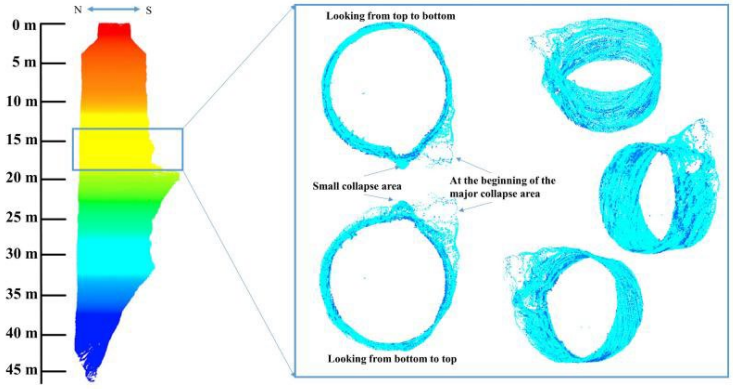

Figure 11: Multi-angle views of the upper deformation area in the coal bunker.

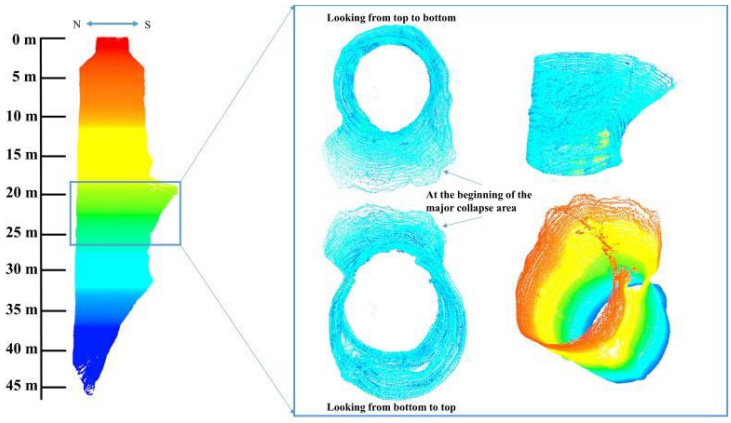

Figure 12: Multi-angle views of the main collapse area in the middle part of the coal bunker.

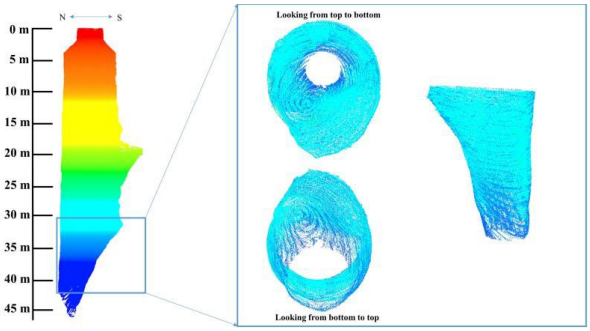

Figure 13: Multi-angle views of the structurally intact area in the lower section of the coal bunker.

ISSN 2616-5767 Vol.7, Issue 3: 29-38, DOI: 10.25236/AJETS.2024.070305

4.3. Comparison with Historical Data

Comparisons with historical data further confirm the system's reliability. Table 2 presents a comparison of the detected damage patterns with previously documented instances. The high degree of correlation between the system's findings and historical records substantiates the system's accuracy in recognizing known damage types and patterns.[25]

Table 2: Coal Bunker Measurement Point Cloud Data Table

Point cloud data		Point 1	Point 2	...	Point n-1	Point n
Subplot(a)	Ground truth	(0.30,5.46)	(0.34,5.46)		(0.39,5.52)	(0.39,5.57)
	Estimated trajectory	(0.28,5.47)	(0.41,5.41)		(0.42,5.53)	(0.44,5.59)
Subplot(b)	Ground truth	(4.73,1.57)	(4.69,1.52)		(4.88,0.97)	(4.92,0.97)
	Estimated trajectory	(4.79,1.56)	(4.65,1.49)		(4.83,0.98)	(4.95,1.00)
Subplot(c)	Ground truth	(0.69,5.93)	(0.69,5.98)		(0.69,5.88)	(0.74,5.88)
	Estimated trajectory	(0.78,5.93)	(0.70,6.00)	⋮	(0.70,5.84)	(0.76,5.83)
Subplot(d)	Ground truth	(1.74,5.59)	(1.74,5.64)		(0.38,3.58)	(0.44,3.58)
	Estimated trajectory	(1.69,5.60)	(1.71,5.67)		(0.43,3.55)	(0.36,3.62)
Subplot(e)	Ground truth	(0.67,6.19)	(0.67,6.23)		(0.72,6.19)	(0.76,6.19)
	Estimated trajectory	(0.66,6.15)	(0.65,6.22)		(0.65,6.20)	(0.84,6.22)
Subplot(f)	Ground truth	(0.74,5.04)	(0.78,5.04)		(0.70,4.96)	(0.70,5.00)
	Estimated trajectory	(0.66,5.03)	(0.82,5.00)		(0.68,4.99)	(0.77,4.99)

The lidar SLAM-enabled detection system enhances safety and efficiency in coal bunker maintenance by mitigating risks for personnel and facilitating targeted repair actions. Early damage detection prevents minor issues from escalating, saving resources and minimizing downtime.

5. Conclusion

This study introduces a novel approach to precisely detect structural damage in coal bunkers by integrating lidar SLAM technology with the Iterative Closest Point (ICP) algorithm. Experimental results highlight the following key findings:

(1) Exceptional Detection Precision: The system demonstrates outstanding trajectory tracking performance, with Absolute Trajectory Error (ATE) and Relative Trajectory Error (RTE) consistently below 0.01, meeting stringent inspection standards.

(2) Versatile Damage Recognition: Diverse critical structural anomalies, such as protruding reinforcement bars and partial wall ruptures, are successfully detected, enabling timely warnings for potential hazards and reliable maintenance decision-making.

(3) Consistency with Historical Data: Detected damage patterns closely align with historical records, verifying accuracy in recognizing known damage types and patterns, while also detecting emerging or evolving damage.

In conclusion, this integrated system offers significant advantages in enhancing detection precision, fortifying safety, and optimizing maintenance processes for coal bunkers. Future research could explore extending this methodology to other underground mine facilities and developing real-time monitoring and warning systems to further advance coal mine safety.

References

[1] Wang Lei. Research and implementation of coal bunker cleaning and anti-blocking technology. Inner Mongolia Coal Economy , 2023, (3): 43-45.
[2] SONG Zhian. Underground coal bunker clearing technology. Mineral Engineering Research, 2010, (5): 59-62.

ISSN 2616-5767 Vol.7, Issue 3: 29-38, DOI: 10.25236/AJETS.2024.070305

[3] Yang Dongdong. Practice on Engineering Technology of Rapid Restoration for Large-range Collapse of Coal Bunker in Mine . Jiangxi Coal Science & Technology, 2023, (2): 75-77.
[4] Tang De-yu. Design improvement of coal bunker lower opening. COAL ENGINEERING, 2021, (5): 9-12.
[5] Jingguo Ma, Zubang Li. Development and application of coal level detection device for shaft bunker. Industry and Mine Automation. 2006; (4): 51-53.
[6] Kajzar V, Kukutsch R, Waclawik P, et al. Innovative approach to monitoring coal pillar deformation and roof movement using 3D laser technology. ISRM EUROCK. ISRM, 2011, (2): 111.
[7] Jiang Q, Zhong S, Pan P Z, et al. Observe the temporal evolution of deep tunnel's 3D deformation by 3D laser scanning in the Jinchuan No. 2 Mine. Tunnelling and Underground Space Technology, 2020, (7): 103237.
[8] Zhou Zhiguo, Cao Jiangwei, Di Shunfan. Overview of 3D Lidar SLAM algorithms. Chinese Journal of Scientific Instrument, 2021, (2): 13-27.
[9] Mendes E, Koch P, Lacroix S. ICP-based pose-graph SLAM, IEEE International Symposium on Safety. Security, and Rescue Robotics (SSRR). IEEE 2016: 195-200.
[10] LOW K L. Linear least-squares optimization for point-to-plane ICP surface registration. University of North Carolina at Chapel Hill; 2004.
[11] SERAFIN J, GRISETTI G. NICP: Dense normal based point cloud registration. Proceedings of the IEEE / RSJ International Conference on Intelligent Robots and Systems. 2014: 742-749.
[12] DESCHAUD J E. IMLS-SLAM: Scan-to-model matching based on 3D data. Proc of IEEE International Conference on Robotics and Automation, 2018.
[13] RUSU R B, BLODOW N, BEETZ M. Fast point feature histograms(FPFH) for 3D registration. IEEE International Conference on Robotics and Automation, IEEE 2009.
[14] CHONG Z J, QIN B, BANDYOPADHYAY T, et al. Mapping with synthetic 2D LIDAR in 3D urban environment. IEEE/RSJ International Conference on Intelligent Robots and Systems, IEEE 2013.
[15] DROESCHEL D, BEHNKE S. Efficent continuous-time SLAM for 3D lidar-based online mapping, IEEE 2018.
[16] LIU Z, ZHANG F. BALM: Bundle adjustment for LiDAR mapping. IEEE Robotics and Automation Letter, 2021: 3184-3191.
[17] SHAN T, ENGLOT B, MEYERS D, et al. LIO-SAM: Tightly-coupled lidar inertial odometry via smoothing and mapping. IEEE/RSJ International Conference on Intelligent Robots and Systems(IROS), IEEE. 2020.
[18] Hornung, A.; Wurm, K.M.; Bennewitz, M.; Stachniss, C.; Burgard, W. OctoMap, An efficient probabilistic 3D mapping framework based on octrees. Auton Robot 34, 2013: 189-206.
[19] Hariharan P, Oreb B F, Brown N. A digital phase-measurement system for real-time holographic interferometry. Optics Communications, 1982: 393-396.
[20] He H, Sun J, Lu Z, et al. Phase-shift laser range finder technique based on optical carrier phase modulation. Applied Optics, 2020: 5079-5085.
[21] Besl P J, McKay N D. Method for registration of 3-D shapes. control paradigms and data structures, 1992: 586-606.
[22] Ezra E, Sharir M, Efrat A. On the performance of the ICP algorithm, Computational Geometry, 2008: 77-93.
[23] Besl P J, Jain R C. Three-dimensional object recognition. ACM Computing Surveys (CSUR), 1985: 75-145.
[24] Kedem G, Watanabe H. Graph-optimization techniques for IC layout and compaction. IEEE transactions on computer-aided design of integrated circuits and systems, 1984: 12-20.
[25] Shamwell E J, Leung S, Nothwang W D. Vision-aided absolute trajectory estimation using an unsupervised deep network with online error correction. 2018 IEEE/RSJ International Conference on Intelligent Robots and Systems (IROS), IEEE 2018: 2524-2531.